

Hierarchical CoS/MoS₂ and Co₃S₄/MoS₂/Ni₂P nanotubes for efficient electrochemical hydrogen evolution in alkaline media

Haifeng Lin,^a Haoyi Li,^b Yanyan Li,^a Junli Liu,^b Xun Wang,^b and Lei Wang^{*a}

^a*College of Chemistry and Molecular Engineering, Qingdao University of Science and Technology, Qingdao 266042, China. E-mail: inorchemwl@126.com*

^b*Key Lab of Organic Optoelectronics and Molecular Engineering, Department of Chemistry, Tsinghua University, Beijing 100084, China*

**Corresponding author. E-mail: inorchemwl@126.com*

Experimental Section

All the chemicals appeared in the synthesis section were purchased from SCRC, Shanghai Co., Ltd., which were of analytic grade and used without further purification.

Synthesis of $\text{Co(OH)}_x(\text{CO}_3)_y$ nanowires: Typically, 0.356 g of $\text{CoCl}_2 \cdot 6\text{H}_2\text{O}$ and 0.068 g of urea were first dissolved in 30 mL water under agitation. Then, the above solution was maintained at 40 °C for 30 min using a water-bath heater. Subsequently, 2.25 mL oleylamine preheated by an oven at 65 °C, was added into the solution under a slow stirring rate to form bigger bluish-green aggregates. Finally, the suspension was transferred to a 40 mL autoclave and kept at 185 °C for 12 h. After reaction, the pink product was washed with water and ethanol by centrifugation for three times before it was dried in a freezing drier.

Synthesis of MoS_2 nanosheets: For the fabrication of MoS_2 nanosheets, firstly, 0.08 g of $(\text{NH}_4)_6\text{Mo}_7\text{O}_{24} \cdot 4\text{H}_2\text{O}$ and 0.15 g of thiourea were added into 30 mL DMF under stirring condition. Then, the suspension was further agitated for 30 min to ensure the complete dissolution of reactants. Following this step, the above solution was transferred to an autoclave and maintained at 200 °C for 24 h. After reaction, the product was washed with ethanol by centrifugation for three times and dried by a freeze-drying method.

Synthesis of CoS hierarchical nanotubes: In a routine preparation, 0.3 g of $\text{Co(OH)}_x(\text{CO}_3)_y$ nanowires were dispersed into 20 mL ethanol by agitation for about 3 min at first. After that, 0.06 g of thiourea was added to the suspension which was further stirred for 20 min. At last, the suspension was sealed in an autoclave and heated at 200 °C for 12 h. The obtained product was rinsed with ethanol by centrifugation for three times before it was dried by lyophilization.

Synthesis of CoS/ MoS_2 hybrid nanotubes: Generally, at first, a calculated amount of prepared CoS nanotubes were dispersed in 30 mL DMF under agitation. Subsequently, 0.08 g of $(\text{NH}_4)_6\text{Mo}_7\text{O}_{24} \cdot 4\text{H}_2\text{O}$ and 0.15 g of thiourea were added into the above suspension, which was then stirred for 30 min before it was sealed in an autoclave. Finally, the autoclave was placed in an oven and heated at 200 °C for 24 h. After reaction, the product was obtained through centrifugal washing with ethanol for three times before the freeze-drying procedure. The product was expressed as CMS_x ($x = 20, 40, \text{ and } 60$), where x represents the calculated loading percentage (wt%) of MoS_2 nanosheets.

Synthesis of CoS/ MoS_2 / Ni(OH)_2 nanotubes and Co_3S_4 / MoS_2 / Ni_2P nanotubes: Regarding the preparation of CoS/ MoS_2 / Ni(OH)_2 nanotubes, in the first place, 0.065 g of $\text{Ni(NO}_3)_2 \cdot 6\text{H}_2\text{O}$, 0.03 g of hexamethylenetetramine, and 0.0065 g of sodium citrate were dissolved in 15 mL water to produce a greenish solution under stirring condition. Meanwhile, 0.02 g of CMS40 was uniformly dispersed into 15 mL water by agitation for about 5 min. Then, the above solution and suspension were mixed together and stirred for 5 min before being transferred to an autoclave. In the end, the autoclave was kept at 100 °C for 6 h in an oven. The product was collected after being rinsed with ethanol for three times and dried by lyophilization. For comparison, pure Ni(OH)_2 nanosheets were also prepared without the addition of CMS40 nanotubes. To get Co_3S_4 / MoS_2 / Ni_2P nanotubes, the synthesized CoS/ MoS_2 / Ni(OH)_2 nanotubes were placed at one end of a ceramic boat, and at the other end of which 0.15 g of $\text{NaH}_2\text{PO}_2 \cdot \text{H}_2\text{O}$ was put. Following this step, the ceramic boat was placed in a tubular furnace with P source against the flow direction of Ar gas, and the Co_3S_4 / MoS_2 / Ni_2P nanotubes can be obtained after calcination

reaction was performed at 350 °C for 2 h using a ramping rate of 5 °C/min.

Characterizations: X-ray diffraction (XRD) measurement was carried out on a Bruker D8 Advance X-ray diffractometer (Cu K α radiation, $\lambda = 1.5418 \text{ \AA}$). Raman spectra were obtained on a LabRAM HR Evolution Raman spectrometer using the exciting light of 532 nm. X-ray photoelectron spectroscopy (XPS) signals were collected by a Thermo Fisher ESCALAB 250 Xi spectrometer using the monochromatic Al K α X-ray source (1486.6 eV) at 2.0 kV and 20 mA. Scanning electron microscopy (SEM) photographs were taken by a Hitachi S5500 Field Emission Gun Scanning Electron Microscope operated at 5 kV. Transmission electron microscopy (TEM), high-resolution TEM (HRTEM), dark-field scanning transmission electron microscopy (STEM), as well as energy dispersive X-ray (EDX) element mapping data were acquired with a FEI Tecnai G2 F20 S-Twin microscope running at 200 kV. Brunauer-Emmett-Teller (BET) specific surface area and corresponding pore-size distribution were examined on a Micromeritics Tristar II 3020 automatic adsorption machine.

Electrochemical Measurements: Electrochemical measurements were performed by the Princeton PARSTAT 4000A work station employing a three-electrode system. The counter electrode and reference electrode was the graphite rod and saturated calomel electrode (SCE), respectively. Meanwhile, 1.0 M KOH aqueous solution was used as the electrolyte for all tests. Before each experiment, 5 mg of catalyst and 1 mg of commercial C were dispersed into a solution composed of 750 μL water and 250 μL ethanol by sonication for 30 min at first; then, 50 μL of Nafion solution (Sigma Aldrich, 5 wt%) was added into the above suspension which was further treated with sonication for another 30 min to form a homogeneous ink. Subsequently, 6 μL of the dispersion was dropped onto a glassy carbon electrode (exposure area of 0.198 cm^2), which was then employed as the working electrode. Linear sweep voltammetry (LSV) curves were collected in the potential range of - 0.9 to - 1.6 V vs. SCE using a scanning rate of 5 $\text{mV}\cdot\text{s}^{-1}$ at room temperature and 1600 rpm. To study the effective surface areas of different catalysts, the corresponding cyclic voltammetry (CV) curves (scanning rate varies from 10 to 60 $\text{mV}\cdot\text{s}^{-1}$) were measured at - 1 to - 0.9 V vs. SCE for $\text{Co}_3\text{S}_4/\text{MoS}_2/\text{Ni}_2\text{P}$ nanotubes, and - 1.1 to - 1 V vs. SCE for CoS/MoS_2 nanotubes, CoS nanotubes, and MoS_2 nanosheets, respectively. The galvanostatic electrochemical impedance spectroscopy (EIS) signals were recorded in the frequency range of 100 kHz to 0.1 Hz, and the amplitude and bias current were set as 0.1 mA and 1 mA, respectively. Cycling stability of the catalyst was investigated by chronoamperometry utilizing the potential at a current density of 20 $\text{mA}\cdot\text{cm}^{-2}$. For the convenience of comparison and data processing, all the potentials vs. SCE were calibrated to a reversible hydrogen electrode (RHE) by adding a value of $(0.242 + 0.059\text{pH})^1$ correspondingly.

Characterization Results

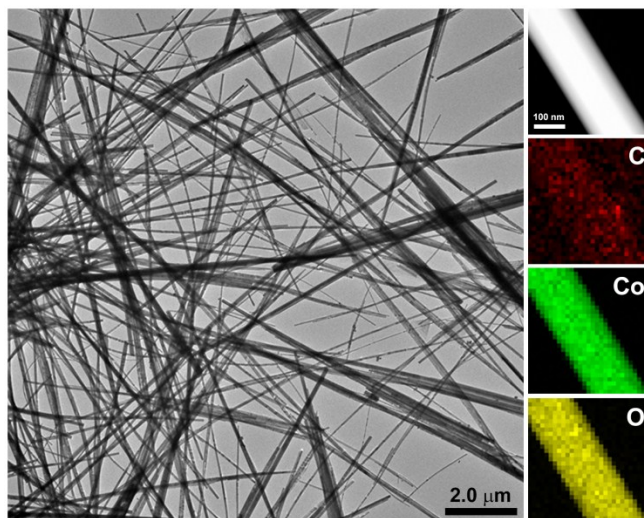


Figure S1. TEM and corresponding STEM and EDX element mapping results of the $\text{Co(OH)}_x(\text{CO}_3)_y$ nanowire precursor.

TEM image of the $\text{Co(OH)}_x(\text{CO}_3)_y$ nanowires template is displayed in Figure S1, which suggests that the nanowires possess a primary diameter of 90~120 nm and a length of about 5~8 μm. Based on the dark-field scanning TEM graph and corresponding energy dispersive X-ray element mapping results of one single nanowire, we can see that all the elements of Co, C, and O have a uniform distribution throughout the whole nanowire.

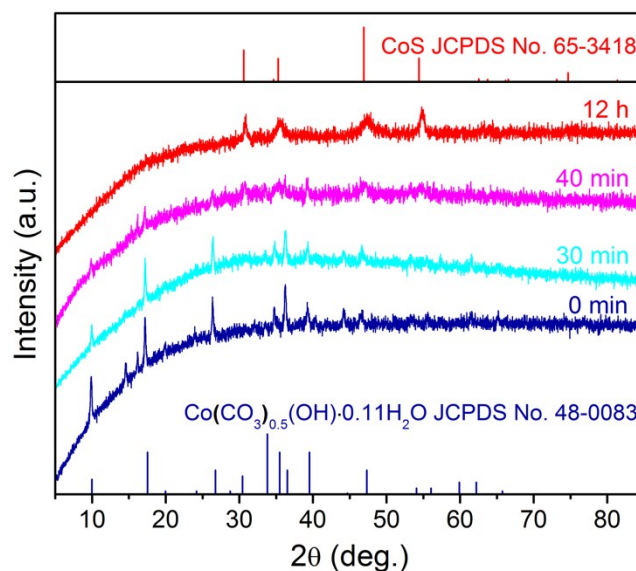


Figure S2. XRD patterns of the products obtained at different sulfidation phases.

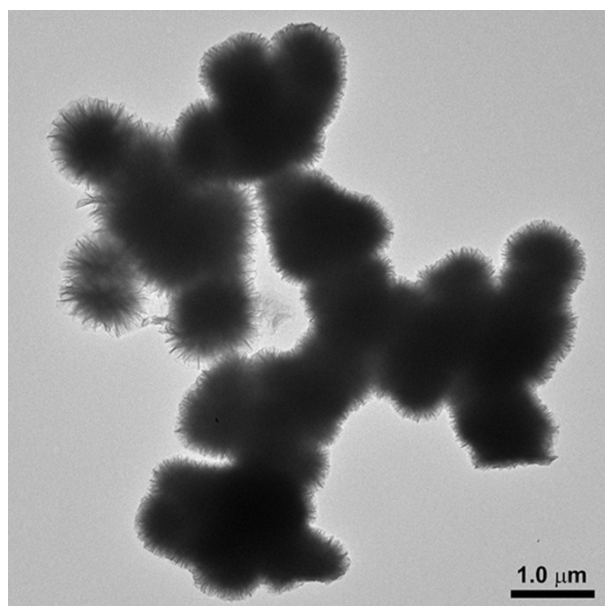


Figure S3. TEM graph of Ni(OH)₂-nanosheet aggregates.

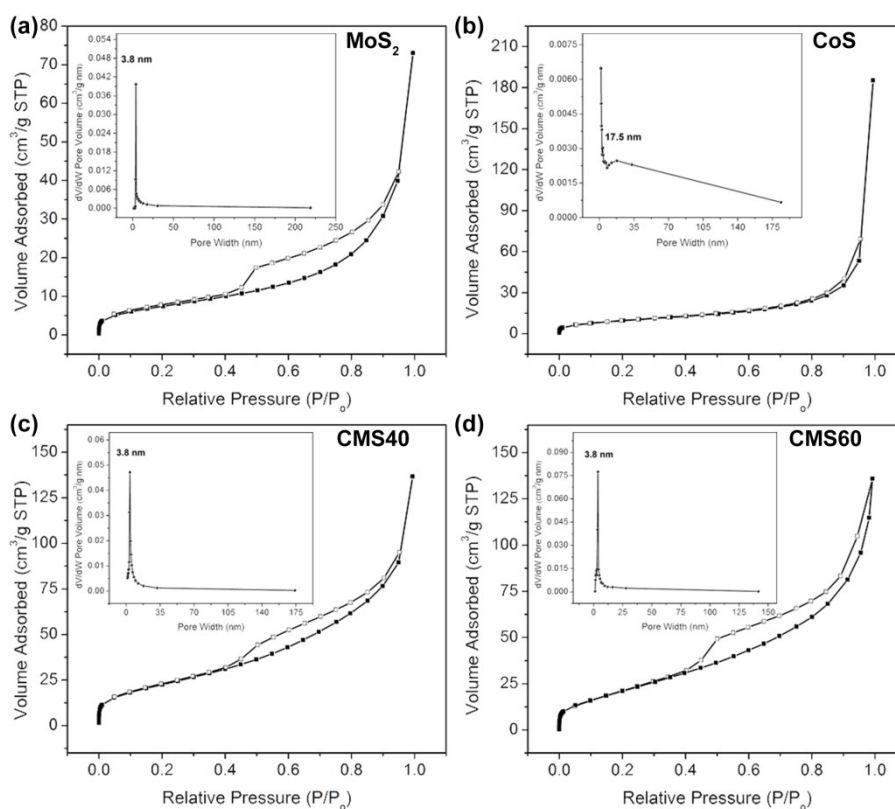


Figure S4. N₂ adsorption-desorption isotherms and corresponding pore-size distributions of (a) MoS₂ nanosheets, (b) CoS nanotubes, (c) CoS/MoS₂ hybrid nanotubes having the MoS₂ loading amount of 40 wt%, (d) CoS/MoS₂ hybrid nanotubes with the MoS₂ loading amount of 60 wt%.

The isotherms and pore-size distributions of MoS₂ nanosheets, CoS nanotubes, CMS40 nanotubes, and CMS60 nanotubes were shown in Figure S4, revealing that all these four samples have a type-III adsorption isotherm with a H3 hysteresis loop. Moreover, the major pore-size

distributions of MoS₂ nanosheets, CMS40 nanotubes, and CMS60 nanotubes are all centered at 3.8 nm, which is smaller than 17.5 nm for CoS nanotubes. According to IUPAC's definition, all these samples could belong to the mesoporous class in view of the related pore-size distributions.

Table S1. ICP and BET results of different electrocatalysts.

Electrocatalysts	MoS ₂ loading amount (wt%)	BET surface area (m ² /g)
MoS ₂ NSs	100	39.6
CoS NTs	0	45.8
CMS20 NTs	17.27	106
CMS40 NTs	35.73	112
CMS60 NTs	54.96	130

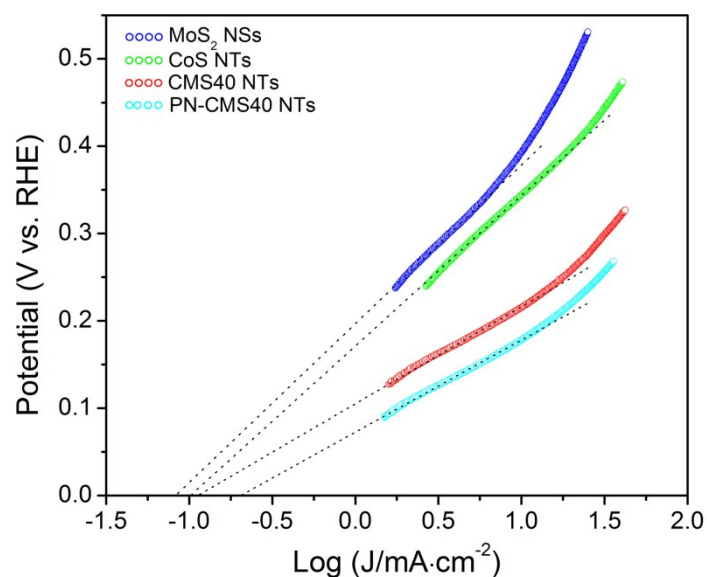


Figure S5. The exchange current densities of different electrocatalysts were determined by the intercepts of corresponding Tafel curves with horizontal axis when the overpotential (V vs. RHE) equals zero.

Table S2. Calculated exchange current densities of varying samples.

Electrocatalysts	Log(J/mA·cm ⁻²) at $\eta = 0$ V	Exchange current density (mA·cm ⁻²)
MoS ₂ nanosheets	-1.07	0.085
CoS nanotubes	-0.99	0.10
CMS40 nanotubes	-0.96	0.11
PN-CMS40 nanotubes	-0.68	0.21

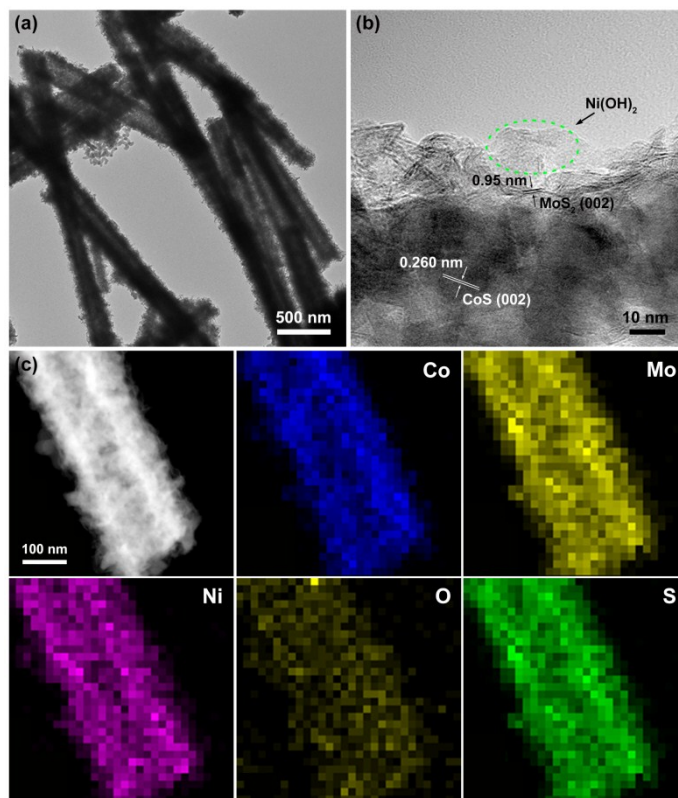


Figure S6. Typical (a) TEM, (b) HRTEM, and corresponding (c) STEM and EDX element mapping results of the composite CoS/MoS₂/Ni(OH)₂ nanotubes.

TEM image of the CoS/MoS₂/Ni(OH)₂ hybrid nanotubes was shown in Figure S6a, which indicates that the nanotubes possess a major diameter of 150~200 nm and a length around 2~5 μm , similar to that of initial CMS40 nanotubes. In order to further analyze the related compositions, HRTEM graph of the hybrid was collected and presented in Figure S6b. We can see that, an enlarged interlayer spacing of 0.95 nm appeared and it could be attributed to the (002) plane of 2H-MoS₂. Meanwhile, the lattice fringes of 0.260 nm were observed, which correspond to the (002) facet of hexagonal CoS. The morphology of Ni(OH)₂ nanosheets (Figure S3) is close to that of MoS₂ nanosheets (Figure 3), hence, it is hard to distinguish the former from the latter. Nevertheless, it is well known that, the crystallinity of metal hydroxides is usually weaker than that of metal sulfides. Consequently, the lying nanosheet marked by the green dashed circle could be recognized as the Ni(OH)₂ nanosheet due to its poor crystallinity. In addition to the HRTEM results, the existence of CoS, MoS₂, and Ni(OH)₂ in this composite was further confirmed by the dark-field STEM and corresponding EDX element mapping measurements (Figure S6c), which clearly demonstrate the tubular distribution of Co, Mo, Ni, O, and S ingredients.

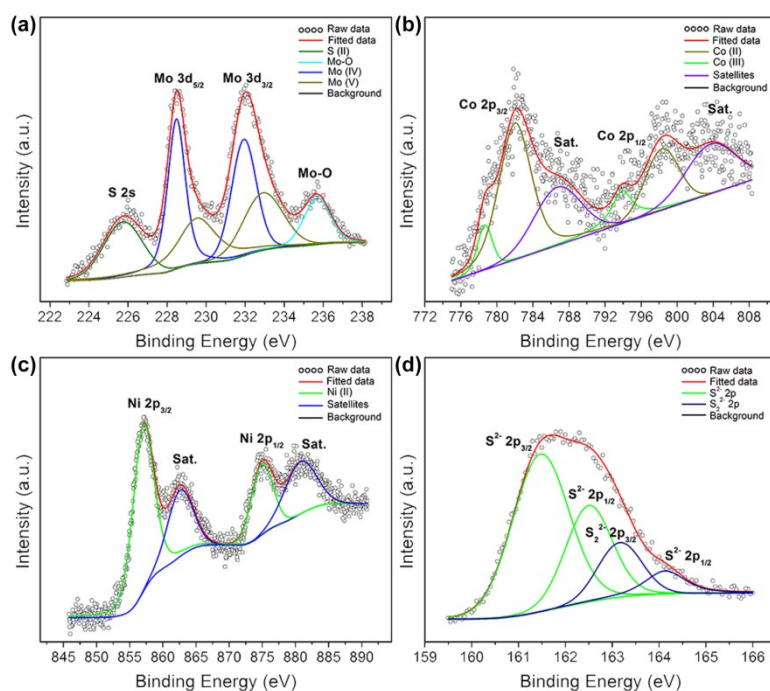


Figure S7. (a) Mo 3d, (b) Co 2p, (c) Ni 2p, and (d) S 2p XPS spectra of CoS/MoS₂/Ni(OH)₂ nanotubes.

The surface element composition and chemical valences of CoS/MoS₂/Ni(OH)₂ nanotubes were investigated by the XPS measurements. As shown in Figure S7a, the main Mo 3d_{5/2} and Mo 3d_{3/2} peaks at 228.5 and 231.9 eV could be related to the Mo⁴⁺ species;² while the adjacent Mo 3d binding energies of 229.5 and 232.9 eV correspond to Mo⁵⁺ state.³ For Co element (Figure S7b), the major Co 2p_{3/2} and Co 2p_{1/2} signals locating at 778.6 and 793.9 eV confirm the formation of Co³⁺ species,⁴ originating probably from the partial surface oxidation of CoS. Correlatively, another set of doublets were observed at 782.1 and 798.5 eV, which are consistent with that of Co²⁺ chemical state.⁵ The spectrum of Ni element was displayed in Figure S7c, in which the binding energies of 857.2 and 875.1 eV were found and they could be ascribed to the 2p_{3/2} and 2p_{1/2} signals of Ni²⁺,⁶ respectively. The binding energies of S 2p_{3/2} and 2p_{1/2} at 161.5 and 162.5 eV were detected (Figure S7d), indicating the presence of S²⁻ species in the hybrid.^{2a} Meanwhile, a set of doublets around 163.2 and 164.1 eV were also discerned from the spectrum, which agree well with that of S₂²⁻ ligands.⁷

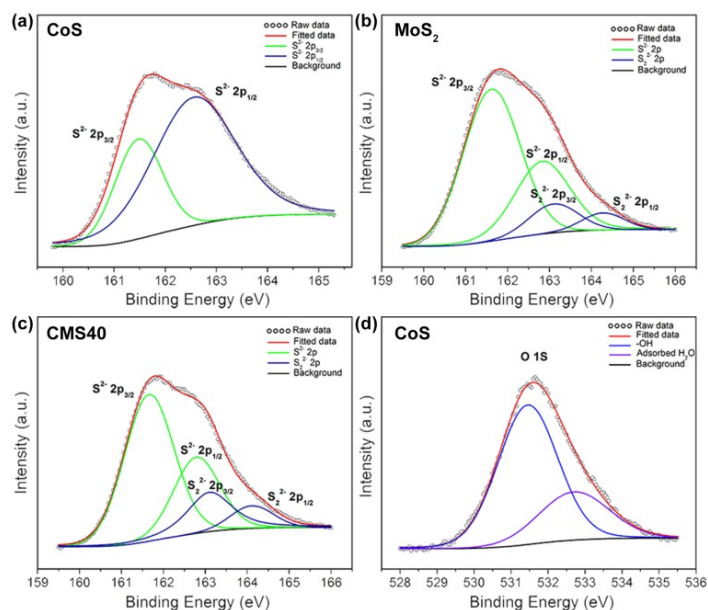


Figure S8. S 2p XPS spectra of (a) CoS nanotubes, (b) MoS₂ nanosheets, and (c) CoS/MoS₂ nanotubes. Presented in (d) is the O 1s signal of CoS nanotubes.

The S 2p_{3/2} and 2p_{1/2} signals of CoS nanotubes were given in Figure S8a, which suggests the presence of S²⁻ species.⁸ On the other hand, the O 1s spectrum shown in Figure S8d reveals that, there are -OH (531.5 eV)⁹ and adsorbed H₂O (532.7 eV)^{2a} existed on the surface of CoS nanotubes. According to the S 2p spectra of individual MoS₂ nanosheets (Figure S8b) and CMS40 nanotubes composite (Figure S8c), two sets of doublets around 161.6-162.8 eV and 163.1-164.2 eV can be found, which are in agreement with that of S²⁻ and S₂²⁻ species, respectively.^{3, 7}

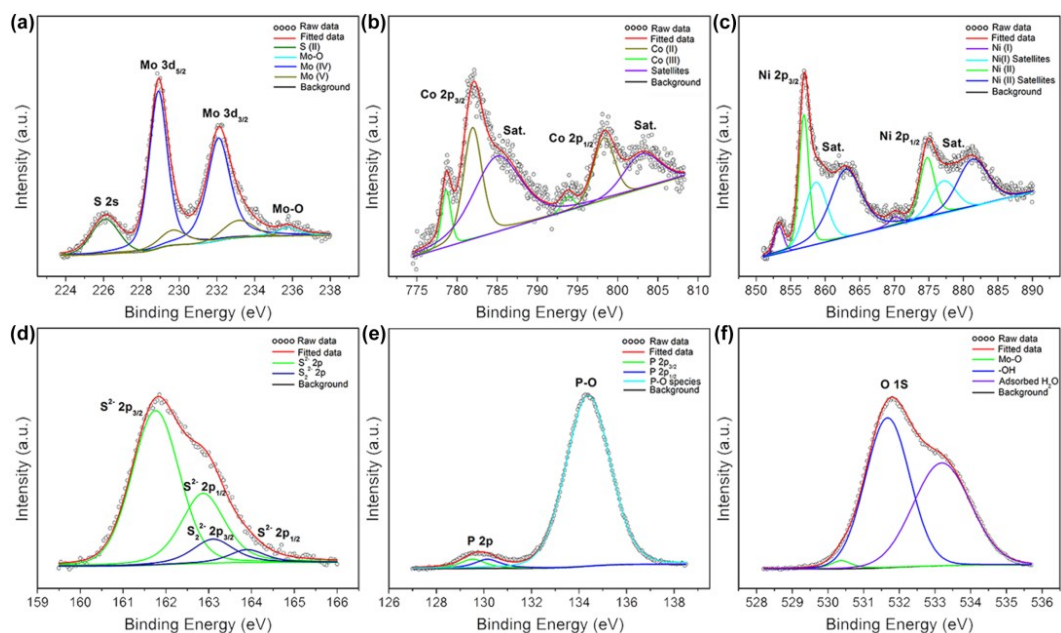


Figure S9. (a) Mo 3d, (b) Co 2p, (c) Ni 2p, (d) S 2p, (e) P 2p, and (f) O 1s XPS spectra of the hybrid Co₃S₄/MoS₂/Ni₂P nanotubes.

The Mo 3d spectrum of $\text{Co}_3\text{S}_4/\text{MoS}_2/\text{Ni}_2\text{P}$ hybrid nanotube was provided in Figure S9a, which indicates that Mo signal involves the compositions stemming from Mo^{4+} (228.9 and 232.1 eV)¹⁰ and Mo^{5+} (229.7 and 233.2 eV)³ species. Meanwhile, a signal around 235.7 eV was found in the spectrum, which evidences the presence of Mo-O bonds.⁷ For Co element (Figure 9b), the binding energies of 778.6-793.9 eV and 782.0-798.3 eV are observed, which can be attributed to the Co^{3+} and Co^{2+} species,⁴⁻⁵ respectively. As shown in Figure S9c, there are two sets of doublets existed in the Ni 2p spectrum, i.e., 853.3-870.2 eV and 856.9-874.7 eV, which could be related to the Ni^+ and Ni^{2+} species,¹¹ respectively. Moreover, the S 2p signal displayed in Figure S9d suggests that, both of S^{2-} (161.7 and 162.8 eV)¹² and S_2^{2-} (163.1 and 163.9 eV)³ species were present in the hybrid. Regarding to P element (Figure S9e), the binding energies at 129.5 and 130.2 can be ascribed to the P 2p_{3/2} and 2p_{1/2} signals,^{1, 13} respectively; while the intense peak situating around 134.3 eV may be resulted from the P-O species.¹³⁻¹⁴ We can find that, the Ni 2p_{3/2} binding energy of Ni_2P (853.3 eV, Figure S9c) is higher than that of metallic Ni (852.2 eV),¹⁵ while the P 2p_{3/2} binding energy (129.5 eV, Figure S9e) is lower than that of elemental P (130.2 eV).¹⁶ Thus, in Ni_2P , the electron transfer between Ni and P happened, and the Ni and P species were provided with a small positive charge (δ^+) and a small negative charge (δ^-), respectively.¹⁷ Based on the O 1s spectrum in Figure S9f, one can conclude that, there are three types of O species including Mo-O (530.3 eV),¹⁸ -OH (531.6 eV),⁹ and adsorbed H_2O (533.2 eV)^{2a} existed on the surface of $\text{Co}_3\text{S}_4/\text{MoS}_2/\text{Ni}_2\text{P}$ nanotubes.

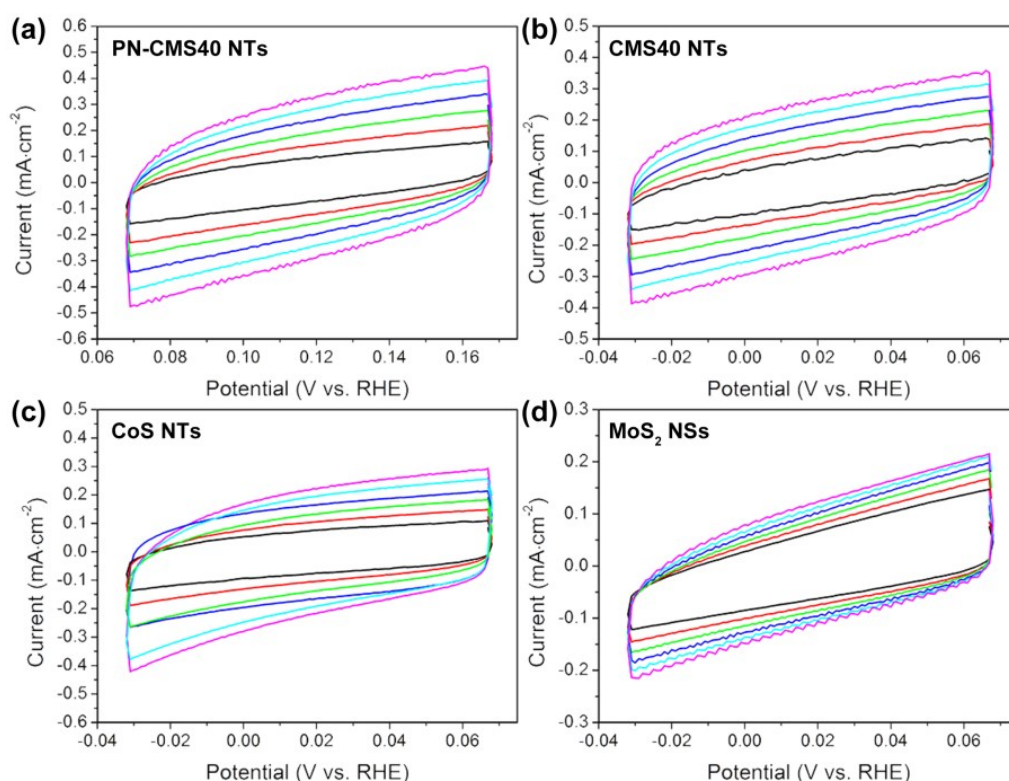


Figure S10. Cyclic voltammetry (CV) curves of different scanning rates (black, 10 $\text{mV}\cdot\text{S}^{-1}$; red, 20 $\text{mV}\cdot\text{S}^{-1}$; green, 30 $\text{mV}\cdot\text{S}^{-1}$; blue, 40 $\text{mV}\cdot\text{S}^{-1}$; cyan, 50 $\text{mV}\cdot\text{S}^{-1}$; purple, 60 $\text{mV}\cdot\text{S}^{-1}$) of (a) $\text{Co}_3\text{S}_4/\text{MoS}_2/\text{Ni}_2\text{P}$ nanotubes, (b) CoS/MoS_2 nanotubes, (c) CoS nanotubes, and (d) MoS_2 nanosheets.

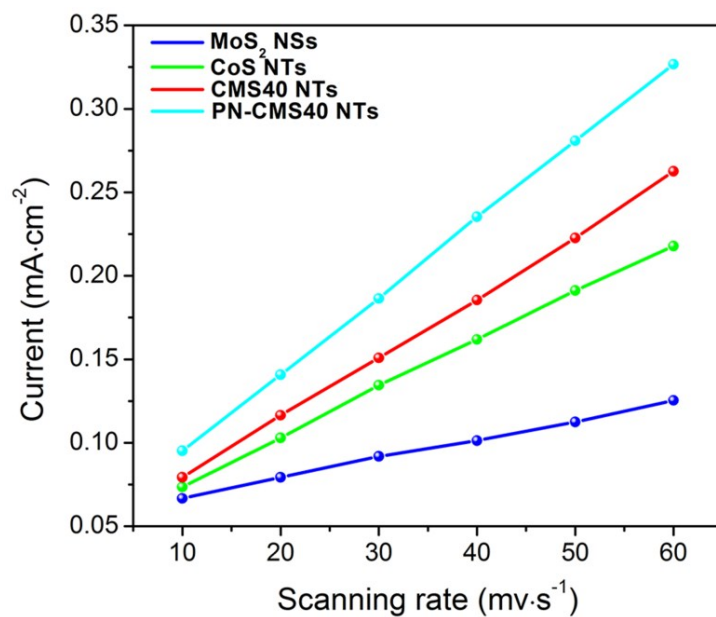


Figure S11. Current densities of the CV curves having different scanning rates at 0.12 V vs. RHE for $\text{Co}_3\text{S}_4/\text{MoS}_2/\text{Ni}_2\text{P}$ nanotubes, and at 0.02 V vs. RHE for CoS/MoS_2 nanotubes, CoS nanotubes, and MoS_2 nanosheets, respectively.

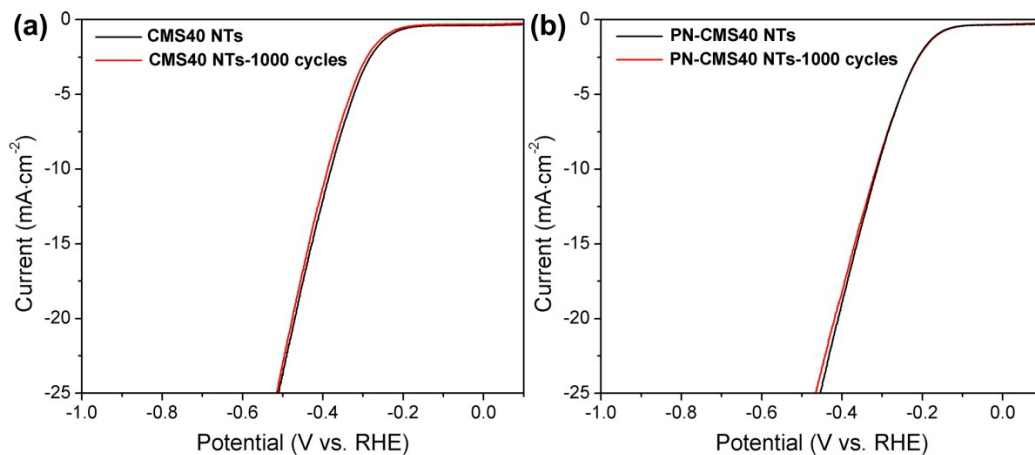


Figure S12. Polarization curves of (a) CMS40 NTs and (b) PN-CMS40 NTs measured in $\text{pH} = 7$ phosphate buffer (0.5 M) initially and after 1000 CV cycles between + 0.2 V and - 0.6 V vs. RHE.

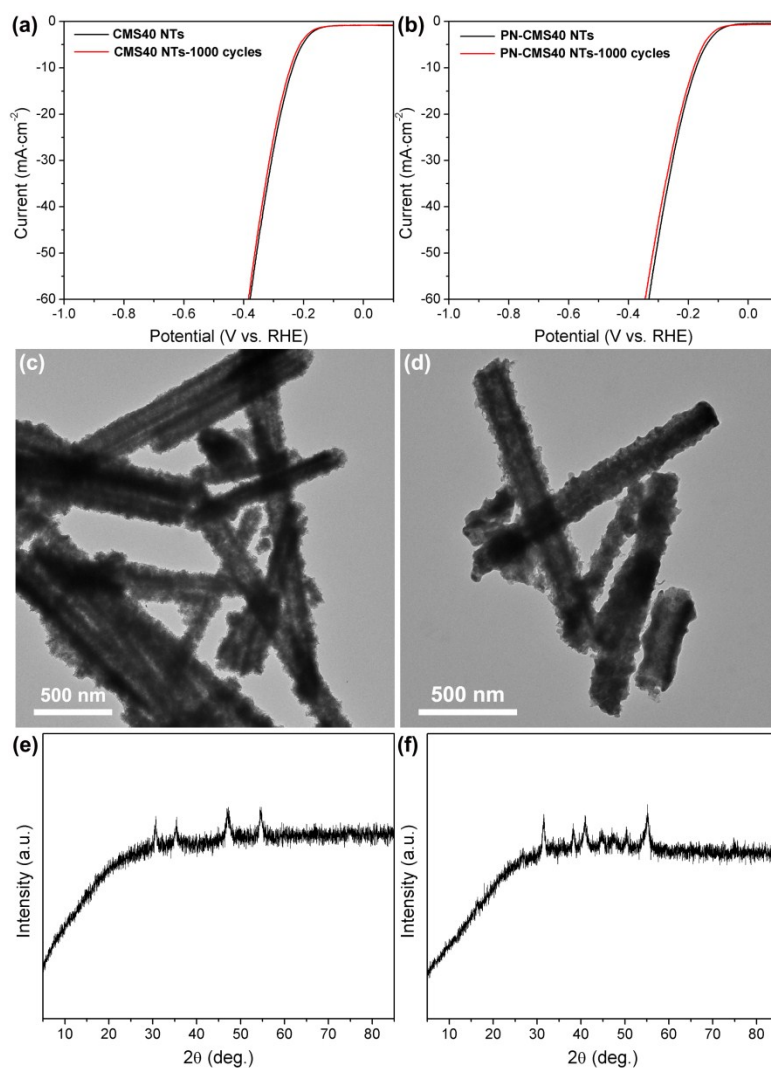


Figure S13. Polarization curves of (a) CMS40 NTs and (b) PN-CMS40 NTs in 1.0 M KOH solution initially and after 1000 CV cycles. The TEM images and XRD patterns of CMS40 NTs and PN-CMS40 NTs after 1000 CV cycles were shown in (c) and (e), and (d) and (f), respectively.

Table S3. Electrocatalytic HER activities of our $\text{Co}_3\text{S}_4/\text{MoS}_2/\text{Ni}_2\text{P}$ nanotubes and catalysts reported by literatures.

Catalyst	Onset η (mV)	η_{10} (mV)	Tafel slope ($\text{mV}\cdot\text{dec}^{-1}$)	J_0 ($\text{mA}\cdot\text{cm}^{-2}$)	Electrolyte	Ref.
$\text{Co}_9\text{S}_8@\text{MoS}_2/\text{CNFs}$	64	190	110	N/A	0.5 M H_2SO_4	19
$\text{Fe}_{0.43}\text{Co}_{0.57}\text{S}_2$	90	220	56	N/A	0.5 M H_2SO_4	20
$\text{Co}_{0.6}\text{Mo}_{1.4}\text{N}_2$	N/A	200	N/A	0.23	0.1 M HClO_4	21
NG/Co-doped C	58	229	126	N/A	0.5 M H_2SO_4	22
Co@NC/NG	49	180	79	N/A	0.5 M H_2SO_4	23
MoSe_2	150	250	80	1.0×10^{-5}	0.1 M H_2SO_4	24
$\text{WS}_{2(1-x)}\text{Se}_{2x}$ NTs	140	260	105	0.029	1 M H_2SO_4	25
$\text{MoS}_2@\text{MoO}_3$	148	240	55	N/A	0.5 M H_2SO_4	26
N,S-doped graphene	130	280	81	N/A	0.5 M H_2SO_4	27

C₃N₄@NG	120	240	52	3.5 x 10 ⁻⁴	0.5 M H ₂ SO ₄	28
C₃N₄ nanoribbons/G	80	207	54	0.040	0.5 M H ₂ SO ₄	29
N,P-doped graphene	215	420	91	2.4 x 10 ⁻⁴	0.5 M H ₂ SO ₄	30
c-CoSe₂/C cloth	80	190	85	N/A	1 M KOH	31
Co-NRCNTs	100	370	N/A	N/A	1 M KOH	32
Mo₂C	120	270	78	4.4 x 10 ⁻³	1 M KOH	33
CoP NWs/C cloth	110	209	129	N/A	1 M KOH	1
Ni(OH)₂/Ni foam	120	250	N/A	N/A	1 M NaOH	34
CoO_x@CN	85	232	115	N/A	1 M KOH	35
MoB	130	220	59	2.0 x 10 ⁻³	1 M KOH	36
WN nanorods array	143	285	170	N/A	1 M KOH	37
NiFe LDH/Ni foam	75	210	N/A	N/A	1 M NaOH	34
Co-P/Co-PO₄	250	380	N/A	N/A	1 M KOH	38
Ni wire	175	318	N/A	N/A	1 M KOH	39
CoS/MoS₂	120	214	106	0.11	1 M KOH	This work
Co₃S₄/MoS₂/Ni₂P NTs	60	178	98	0.21	1 M KOH	This work

Abbreviations: CNFs, carbon nanofibers; Co-NRCNTs, cobalt-embedded nitrogen-rich carbon nanotubes; NC, nitrogen-doped carbon; G, graphene; NG, nitrogen-doped graphene; LDH, layered double hydroxide; CN, N-doped carbon; NTs, nanotubes; NWs, nanowires.

References:

- 1 J. Q. Tian, Q. Liu, A. M. Asiri and X. P. Sun, *J. Am. Chem. Soc.*, 2014, **136**(21), 7587-7590.
- 2 a) J. F. Xie, J. J. Zhang, S. Li, F. Grote, X. D. Zhang, H. Zhang, R. X. Wang, Y. Lei, B. C. Pan and Y. Xie, *J. Am. Chem. Soc.*, 2013, **135**(47), 17881-17888; b) D. Merki, S. Fierro, H. Vrubel and X. L. Hu, *Chem. Sci.*, 2011, **2**(7), 1262-1267.
- 3 J. H. Xiong, Y. H. Liu, D. K. Wang, S. J. Liang, W. M. Wu and L. Wu, *J. Mater. Chem. A*, 2015, **3**(24), 12631-12635.
- 4 Y. F. Zhang, C. C. Sun, H. Q. Su, W. Huang and X. C. Dong, *Nanoscale*, 2015, **7**(7), 3155-3163.
- 5 Z. F. Zeng, D. Z. Wang, J. L. Zhu, F. Q. Xiao, Y. D. Li and X. H. Zhu, *CrystEngComm*, 2016, **18**(13), 2363-2374.
- 6 D. U. Lee, J. Fu, M. G. Park, H. Liu, A. G. Kashkooli and Z. W. Chen, *Nano Lett.*, 2016, **16**(3), 1794-1802.
- 7 Y. H. Chang, R. D. Nikam, C. T. Lin, J. K. Huang, C. C. Tseng, C. L. Hsu, C. C. Cheng, C. Y. Su, L. J. Li and D. H. C. Chua, *ACS Appl. Mater. Interfaces*, 2014, **6**(20), 17679-17685.
- 8 S. H. Chang, M. D. Lu, Y. L. Tung and H. Y. Tuan, *ACS nano*, 2013, **7**(10), 9443-9451.
- 9 J. Zhang, L. P. Li, T. J. Yan and G. S. Li, *J. Phys. Chem. C*, 2011, **115**(28), 13820-13828.
- 10 P. L. He, H. Y. Li, H. L. Liu and X. Wang, *ChemNanoMat*, 2016, **2**(7), 665-670.
- 11 J. Zhang, T. Wang, P. Liu, Z. Liao, S. Liu, X. Zhuang, M. Chen, E. Zschech and X. Feng, *Nat. Commun.*, 2017, **8**, 15437.
- 12 P. P. Wang, H. Y. Sun, Y. J. Ji, W. H. Li and X. Wang, *Adv. Mater.*, 2014, **26**(6), 964-969.
- 13 A. Han, H. L. Chen, Z. J. Sun, J. Xu and P. W. Du, *Chem. Commun.*, 2015, **51**(58), 11626-11629.

- 14 H. Li, P. F. Yang, D. S. Chu and H. X. Li, *Appl. Catal. A-Gen.*, 2007, **325**(1), 34-40.
- 15 Y. Pan, Y. Q. Liu, Y. Lin and C. G. Liu, *ACS Appl. Mater. Interfaces*, 2016, **8**(22), 13890-13901.
- 16 Y. Pan, Y. Lin, Y. J. Chen, Y. Q. Liu and C. G. Liu, *J. Mater. Chem. A*, 2016, **4**(13), 4745-4754.
- 17 Q. Liu, J. Q. Tian, W. Cui, P. Jiang, N. Y. Cheng, A. M. Asiri and X. P. Sun, *Angew. Chem.*, 2014, **126**(26), 6828-6832.
- 18 Y. M. Sun, X. L. Hu, W. Luo and Y. H. Huang, *ACS nano*, 2011, **5**(9), 7100-7107.
- 19 H. Zhu, J. F. Zhang, R. P. Yan Zhang, M. L. Du, Q. F. Wang, G. H. Gao, J. D. Wu, G. M. Wu, M. Zhang, B. Liu, J. M. Yao and X. W. Zhang, *Adv. Mater.*, 2015, **27**(32), 4752-4759.
- 20 D. S. Kong, J. J. Cha, H. T. Wang, H. R. Lee and Y. Cui, *Energy Environ. Sci.*, 2013, **6**(12), 3553-3558.
- 21 B. F. Cao, G. M. Veith, J. C. Neufeind, R. R. Adzic and P. G. Khalifah, *J. Am. Chem. Soc.*, 2013, **135**(51), 19186-19192.
- 22 Y. Hou, Z. H. Wen, S. M. Cui, S. Q. Ci, S. Mao and J. H. Chen, *Adv. Funct. Mater.*, 2015, **25**(6), 872-882.
- 23 W. J. Zhou, J. Zhou, Y. C. Zhou, J. Lu, K. Zhou, L. J. Yang, Z. H. Tang, L. G. Li and S. W. Chen, *Chem. Mat.*, 2015, **27**(6), 2026-2032.
- 24 F. H. Saadi, A. I. Carim, J. M. Velazquez, J. H. Baricuatro, C. C. L. McCrory, M. P. Soriaga and N. S. Lewis, *Acs Catal.*, 2014, **4**(9), 2866-2873.
- 25 K. Xu, F. M. Wang, Z. X. Wang, X. Y. Zhan, Q. S. Wang, Z. Z. Cheng, M. Safdar and J. He, *ACS nano*, 2014, **8**(8), 8468-8476.
- 26 Z. B. Chen, D. Cummins, B. N. Reinecke, E. Clark, M. K. Sunkara and T. F. Jaramillo, *Nano Lett.*, 2011, **11**(10), 4168-4175.
- 27 Y. Ito, W. T. Cong, T. Fujita, Z. Tang and M. W. Chen, *Angew. Chem. Int. Edit.*, 2015, **54**(7), 2131-2136.
- 28 Y. Zheng, Y. Jiao, Y. H. Zhu, L. H. Li, Y. Han, Y. Chen, A. J. Du, M. Jaroniec and S. Z. Qiao, *Nat. Commun.*, 2014, **5**, 3783.
- 29 Y. Zhao, F. Zhao, X. P. Wang, C. Y. Xu, Z. P. Zhang, G. Q. Shi and L. T. Qu, *Angew. Chem.-Int. Edit.*, 2014, **53**(50), 13934-13939.
- 30 Y. Zheng, Y. Jiao, L. H. Li, T. Xing, Y. Chen, M. Jaroniec and S. Z. Qiao, *ACS nano*, 2014, **8**(5), 5290-5296.
- 31 P. Z. Chen, K. Xu, S. Tao, T. P. Zhou, Y. Tong, H. Ding, L. D. Zhang, W. S. Chu, C. Z. Wu and Y. Xie, *Adv. Mater.*, 2016, **28**(34), 7527-7532.
- 32 X. X. Zou, X. X. Huang, A. Goswami, R. Silva, B. R. Sathe, E. Mikmeková and T. Asefa, *Angew. Chem.-Int. Edit.*, 2014, **126**(17), 4461-4465.
- 33 C. G. Morales-Guio, K. Thorwarth, B. Niesen, L. Liardet, J. Patscheider, C. Ballif and X. L. Hu, *J. Am. Chem. Soc.*, 2015, **137**(22), 7035-7038.
- 34 J. S. Luo, J. H. Im, M. T. Mayer, M. Schreier, M. K. Nazeeruddin, N. G. Park, S. D. Tilley, H. J. Fan and M. Grätzel, *Science*, 2014, **345**(6204), 1593-1596.
- 35 H. Jin, J. Wang, D. Su, Z. Wei, Z. Pang and Y. Wang, *J. Am. Chem. Soc.*, 2015, **137**(7), 2688-2694.
- 36 H. Vrubel and X. L. Hu, *Angew. Chem.-Int. Edit.*, 2012, **124**(51), 12875-12878.
- 37 J. L. Shi, Z. H. Pu, Q. Liu, A. M. Asiri, J. M. Hu and X. P. Sun, *Electrochim. Acta*, 2015, **154**, 345-351.
- 38 Y. Yang, H. L. Fei, G. D. Ruan and J. M. Tour, *Adv. Mater.* 2015, **27**(20), 3175-3180.
- 39 J. R. McKone, B. F. Sadtler, C. A. Werlang, N. S. Lewis and H. B. Gray, *Acs Catal.*, 2013, **3**(2), 166-169.

